Co-located wind and temperature observations at mid-latitudes during mesospheric inversion layer events

A. Mariaccia[1], P. Keckhut[1], A. Hauchecorne[1], S. Khaykin[1], and M. Ratynski[1]

[1]Laboratoire Atmosphères, Milieux, Observations Spatiales, UMR 8190, Institut Pierre-Simon Laplace, Université Versailles-Saint Quentin, Université Paris-Saclay, 78280 Guyancourt, France.

Key Points:

- First simultaneous wind and temperature observations in the altitude range 30-90 km during mesospheric inversion layer events.
- According to these new observations, there is a strong wind deceleration occurring at the same altitude that the temperature inversion.
- These results argue in favor of the MIL's formation mechanism involving gravity wave dissipation.

Corresponding author: Alexis Mariaccia, `alexis.mariaccia@latmos.ipsl.fr`

Abstract

[The mesospheric inversion layer (MIL) phenomenon refers to a temperature enhancement (10-50 K) in a vertical layer (~10 km) lasting several days and spanning thousands of kilometers within the mesosphere. As MILs govern the mesospheric variability, their study is crucial for a better understanding of the middle-atmosphere global circulation and applications in aeronautics since perturbations in the mesosphere are significant issues for the safe reentry of rockets, space shuttles, or missiles. However, the description of this phenomenon remains partial, as no observations of MIL's effects on winds exist, preventing a complete understanding of the mechanisms responsible for their formation. Here, we first report an investigation of simultaneous wind-temperature observations in the altitude range of 30-90 km during MIL events. As a result, the profiles exhibit a strong winds deceleration occurring in the same altitude range that the temperature inversion, confirming the role of gravity waves in MIL's formation mechanisms.]

Plain Language Summary

[In the atmosphere, waves propagate from the lower to upper layers, transferring their momentum to the medium. The mesosphere (50-90 km) is subject to these energy transfers causing unexpected temperature increases (10-50 K) over a vertical layer (~10 km). These deviations are named mesospheric inversion layers (MILs). Though largely observed in temperature profiles, the MIL phenomenon is partially misunderstood as MIL's impacts on the wind in the middle atmosphere remain unknown. In this study, we first provide observed simultaneous wind-temperature profiles between 30 and 90 km during MIL events. We found a strong wind deceleration in the same altitude range where the temperature increases. This result argues in favor of the role of gravity waves in MIL's formation mechanisms.]

1 Introduction

The mesosphere (50-90 km) is a substantial layer where large and small-scale perturbations occur, essentially due to the propagation and the breaking of atmospheric tides and waves from sources above and below, inducing deviations from its natural thermal structure. Among these perturbations, the so-called Mesospheric Inversion Layer (MIL) is now recognized to be responsible for a large part of the mesospheric variability. Additionally, since mesospheric perturbations are significant issues for applications in aeronautics and particularly the safe reentry of space shuttles and missiles (Wing et al., 2020), MILs have aroused large interest. Indeed, since the first MIL phenomenon's signatures observed by rockets (e.g., Stroud et al., 1960; Theon et al., 1967; Schmidlin, 1976), reporting a non-expected positive lapse rate in the mesosphere, numerous observations, and studies of MIL events have been performed, regularly documenting the advances on this topic (e.g., Leblanc & Hauchecorne, 1997; Gan et al., 2012; Dao et al., 1995; Duck et al., 2001; Leblanc et al., 1995; Cutler et al., 2001). An important review of the knowledge state on the MIL phenomenon has been carried out by Meriwether and Gardner (2000). At first, the MIL is defined as a layer of about 10 km with enhanced temperature between 15 and 50 K, spanning over a thousand square kilometers over several days. Currently, MILs are known to occur quite often at low to mid-latitudes, preferentially in winter, and have been separated into two subtypes: the lower MIL, occurring between 65 and 80 km, especially in winter, and the upper MIL, occurring above 85 km. Different mechanisms have been suggested to explain their formation: planetary waves dissipation (Salby et al., 2002; France et al., 2015), gravity waves and tides interaction (Liu & Hagan, 1998; Meriwether & Gardner, 2000) or chemical heating (Meriwether & Mlynczak, 1995; Ramesh et al., 2013), but they remain not entirely described and are still an active research field. Among the missing information in the description of the MIL phenomenon, the wind behavior in the whole middle atmosphere (30-90 km) when a MIL event occurs remains an unanswered question even though several studies have suggested its significant role in the MIL appearance (Meriwether & Gerrard, 2004). For instance, Hauchecorne et al. (1987), who estimated the role of gravity wave dissipation in the MIL's persistence, shows that this process strongly depends on the temperature and the background wind. On the other hand, Salby et al. (2002) and Sassi et al. (2002), focusing on the mechanism of MIL creation, have revealed with simulations that the planetary wave breaking is supposed to occur in the same altitude range of a weak zonal wind region. Therefore, this question is a substantial stake in understanding the MIL phenomenon and, more broadly, the impacts on general middle atmosphere circulation. Although some studies have reported simultaneous wind-temperature observations in the middle atmosphere (e.g., Stroud et al., 1960; Theon et al., 1967; Baumgarten, 2010), most of them did not focus on the MIL phenomenon, while sometimes detecting a MIL without knowing the phenomenon, and therefore did not lead to further wind observations in the frame of the MIL study. For instance, Stroud et al. (1960), unaware of the MIL phenomenon, reported a temperature inversion at 80 km with strong wind shear at the same altitude without giving any explanation to this observed behavior.

Despite this supposed role, among studies focusing on MILs, only simultaneous zonal wind and temperature observations from Na LiDAR in the altitude range 85-100 km have been reported in Huang et al. (1998, 2002) who detected a large wind shear associated with a MIL. However, more than this partial description of the wind signature at upper MIL altitudes is required to determine the entire shear profile or study how gravity waves propagate from the stratosphere to the thermosphere (Le Du et al., 2022).

Consequently, all the theoretical and modeled wind behavior assumptions in the middle atmosphere during a MIL event have never been confirmed due to the absence of accurate co-located and simultaneous temperature and wind measurements in this part of the atmosphere. The main reason was the challenge of measuring winds accurately across this wide range of altitudes with the former instruments (Meriwether & Gerrard, 2004). To our knowledge, the DYANA campaign, which took place in the northern hemisphere in 1990, is one the rare campaign during which Rayleigh LiDAR and falling spheres simultaneously measured temperature and wind, respectively, in the whole middle atmosphere. However, the characteristics of the MILs observed during this campaign were not studied as this was not one of the main objectives and are therefore revealed for the first time in this study. Since then, and as the falling sphere profiles suffer from significant smoothing and bias (see here Fig. 1) due to the large speed of the payload in the mesosphere, making this technique, not enough reliable (Lübken et al., 1994), the remote sensing techniques have been developed, particularly with the rise of the Doppler Rayleigh LiDAR technology capable of accurately measuring the temperature and wind in the atmospheric window of 30-90 km. Such LiDAR currently operates at the Observatoire of Haute-Provence (OHP) in addition to the Rayleigh LiDAR and Ozone LiDAR, measuring the temperature and monitoring the ozone, respectively, making the OHP one of the rare station in the world where co-located and simultaneous wind-temperature observations in the middle-atmosphere are possible.

In this context, our study aims to answer how the winds evolve during MIL events by providing the first time simultaneous temperature and wind observations acquired at two locations in the south of France in the altitude range of 30-90 km. The two observation data sets used here were acquired at Biscarrosse during the DYANA campaign in 1990 and at the OHP, located 550 km apart, in 2021/2022 winter. As Biscarrosse and OHP stations exhibit a similar mesospheric climatology (Hauchecorne et al., 1991), it is interesting to investigate the MIL's signature at both sites. Additionally, we explored how ERA5 reanalyses simulated the wind and temperature during MIL events.

The publication is structured as follows. In Section 2, the data set from DYANA and Aeolus Validation campaigns as well as ERA5 reanalyses are presented. Then, the method to identify and to characterize MIL events is described in Section 3. Afterward, the temperature-wind observations for each selected date with MIL events are shown and commented in Section 4. Finally, mechanisms responsible for lower MILs are discussed, and perspectives are given in Section 5.

2 Data description

2.1 The DYANA Campaign: Rayleigh LiDAR and Falling Spheres

The DYANA (DYnamics Adapted Network for the Atmosphere) campaign was conducted in the northern hemisphere over a large horizontal area from January to March 1990 in order to explore the middle atmosphere dynamics (10-100 km). The DYANA campaign was designed to improve the lack of horizontal coverage missing during previous campaigns. The main dynamical objectives were to study the large, medium, and small-scale variations generated by planetary waves, gravity waves, tides, and turbulence. Another aim was to inter-compare measurements in order to cross-check experimental methods. Thus, several techniques were employed during these three months to measure temperature and density from multiple ground-based stations. The set of these techniques with their monitored height range was: rocket bornes (90-115 km), falling spheres (30-90 km), Rayleigh LiDAR (30-90 km), sodium LiDAR (80-105 km), data sondes (25-65 km) and radiosondes (0-32 km). Coordinated temperature and density measurements were occasionally performed from different instruments at the exact location and approximately the same periods (about 1h) to perform inter-comparisons. For instance, the station based in southwest France at Biscarrosse (44°N-1°W) benefited from simultaneous observations from Rayleigh LiDAR and falling spheres. During the campaign, falling spheres were released at about 110 km altitude to obtain, from the radar position information, density, temperature, and winds profiles in the middle atmosphere. A detailed description of the falling sphere technique can be found in Engler (1965) and Jones and Peterson (1968). At the ground, a Rayleigh LiDAR measured the density profile by counting the number of photons, and then the temperature was inferred by assuming hydrostatic equilibrium in the 30-90 km range, where a pure molecular backscattering is expected. The vertical resolution of LiDAR temperature profiles is typically 200 m. The Rayleigh Lidar method and the technical information about the LiDAR located at Biscarrosse have been described in Hauchecorne et al. (1991). The complete description of the DYANA campaign and its objectives have been reported in Offermann (1994). The presentation of each instrumental technique and the inter-comparison results are shown in Lübken et al. (1994). In the measurements data set carried out at Biscarrosse in 1990, eight dates of co-located and simultaneous temperature-wind observations are available.

2.2 Aeolus Validation Campaign: OHP LiDARs

In August 2018, in the frame of the Living Planet Program, Aeolus satellite was launched by the European Space Agency (ESA) in order to provide global wind profiles from the surface to 30 km for a three years period (Straume, A.G. et al., 2020). The Aeolus satellite measures horizontal line-of-sight (HLOS) winds with a Doppler wind LiDAR named ALADIN (Atmospheric LAser Doppler Instrument) which is the first ever Doppler Wind LiDAR (DWL) embarked on a satellite. In the meantime and in order to assess and to validate Aeolus wind observations, ground-based Doppler LiDAR observations within the AboVE-2 (Aeolus Validation Experiment) were undertaken at the Observatory of Haute-Provence (OHP, 44°N, 6°E) (Ratynski et al., 2022) where the double-edge technique for wind profiling, which is realized in ALADIN Rayleigh channel, was first demonstrated (Chanin et al., 1989; Garnier et al., 1992). For decades, several co-located LiDARs have been monitoring the middle atmosphere at the OHP within the Network for the Detection of Composition Changes (NDACC). Since 1993, a LIOvent Doppler LiDAR has been measuring the wind velocities at OHP providing the first lidar-based wind climatology in the middle atmosphere (Souprayen et al., 1999). The principle, using the Rayleigh backscattering at 532 nm, is based on the Doppler shift between the emitted and the backscattered laser light caused by the displacement of scattering molecules relative to the LiDAR. The detection of Doppler shift is performed employing a double-edge Fapbry-Perot interferometer. The complete description of the Doppler LiDAR's technique and the instrument design at OHP has been reported in Chanin et al. (1989) and more recently in Khaykin et al. (2020).

Finally, an Ozone LiDAR has been monitoring the ozone as part of the Network for the Detection of Stratospheric Changes (NDSC). The Ozone LiDAR's principle rests on the DIAL (DIfferential Absorption Lidar) technique requiring the emission of two simultaneous laser wavelengths, 308 (absorbing) and 355 (non-absorbing) nm here, with differential absorption by ozone to provide its vertical profile. The method and the technical information about the Ozone LiDAR at OHP have been described in several studies (e.g., Godin-Beekmann et al., 2003; Wing et al., 2018). Thus, in order to perform simultaneous wind and temperature measurements at OHP, the temperature observations can also be derived by the Ozone LiDAR in off mode by using only the non-absorbing channel (355 nm). Therefore, in addition to the dataset from the DYANA campaign, we benefited from 44 dates of simultaneous observations of temperature and wind carried out at the OHP from 2018 to 2022.

2.3 ERA5 Reanalyses

The ERA5 reanalyses are the last generation of reanalyses, archiving the past climate on earth from 1950 to the present, produced by the ECMWF (European Center Medium for Weather Forecast) since 2016. These ERA5 reanalyses are produced with a 4DVar assimilation scheme and the integrated system forecast (IFS) Cycle 41r2. The ERA5 output is constructed every hour on a 0.25° latitude-longitude grid and 137 vertical levels lying from the surface to the level pressure 0.01hPa (approximately 80 km). More technical information about ERA5 reanalyses can be found in Hersbach et al. (2020). Here, in order to pursue investigations on how the ECMWF model simulates the MIL phenomenon already undertaken in Mariaccia et al. (2022), ERA5 wind and temperature reanalyses are extracted at the nearest hour of the mid of acquisitions for the six dates shown above Biscarrosse and the OHP (Fig. 1 and 2).

3 Method for identifying and characterizing MILs

Here, in order to identify MIL events within the temperature profiles, we followed the method developed by Leblanc and Hauchecorne (1997) and Fechine et al. (2008), which has been applied in numerous previous studies (e.g., Cutler et al., 2001; Leblanc et al., 1998; Ardalan et al., 2022). According to them, a MIL is identified when these three criteria are observed:

- The MIL bottom must be at least 5 km above the stratopause and the MIL top below 90 km.
- The temperature perturbation must be significant relative to the measurement uncertainty, i.e., Terr $< \Delta$T.
- Finally, the temperature amplitude must be 2σ larger than the temperature fluctuations expected by gravity waves at these altitudes. According to Mzé et al. (2014), gravity waves are expected to generate perturbations of 1.6 K at 50 km and 4 K at 75 km.

Afterward, we characterized each observed MIL by computing their amplitude, thickness, and gradient similarly to the method developed in Ardalan et al. (2022) (see their Figure 2). Thus, for each observed temperature profile, our algorithm identified two altitudes: the altitude of the bottom MIL from which the temperature gradient reverses and the altitude of the top MIL where the temperature maximum is reached. These two altitudes are pointed out with horizontal solid lines in Figures 1 and 2 delimiting the observed MIL's altitude range (ΔZ_{MIL}). Finally, the altitude corresponding to the potential extension of the temperature anomaly is determined when the temperature profile returns to the standard climatology which is determined somehow arbitrarily. Thus, amplitudes of temperature increase (ΔT) within the MIL is computed over the ΔZ_{MIL} thickness (Fig. 1) for each profile. As the reversal of temperature gradients remains a better indicator than a wind drop to identify MILs and since observed wind drop occurs around where temperature rises, zonal (ΔU) and meridional (ΔV) wind deviations caused by these temperature inversions are also calculated over the thickness ΔZ_{MIL}.

4 Results

4.1 DYANA campaign in Biscarrosse

As a result, only two dates in the data from the DYANA campaign possess lower MIL presences which are exploitable. Figure 1 shows temperature zonal and meridional wind profiles measured by LiDAR and falling spheres. Simulated temperature profiles are provided by ERA5 for these two cases in the middle atmosphere during which lower MILs were present. According to these profiles, it is evident that a connection exists between the temperature and wind evolutions, i.e., a wind deceleration occurs, sometimes leading to a wind reversal for both meridional and zonal winds when the temperature increases. Moreover, this wind deceleration tends to start at an altitude around the altitude where the temperature inversion starts. For instance, the MIL observed on 18 Jan 1990 illustrates very well this behavior with a temperature increase of 13.6 ± 0.8 K, causing the deceleration of the total wind lying from 92 m.s^{-1} to 12 m.s^{-1}. While, for the MIL observed on 5 Feb 1990, a lower deceleration of the total wind is found lying from 51 m.s^{-1} to 37 m.s^{-1} for a temperature elevation of 24.4 ± 3 K. Thus, according to these results, the magnitude of the wind deceleration is not necessarily linearly linked with the temperature amplitude of the MIL. However, since the method to compute the wind decrease is based on the vertical domain where the temperature positive gradient is observed and not in the altitude range where the observed wind really started and finished to decelerate, these results possess some uncertainties on calculated values. Nevertheless, this method allows to capture the wind deceleration process occurring during a MIL phenomenon.

The temperature measured by the falling sphere are compared with the collocated LiDAR temperature profile for the same dates. As a result, falling spheres' temperatures are systematically lower than LiDAR temperatures between 65 and 70-75 km for the two dates. Lübken et al. (1994) have reported that this difference is about 5 K between 65 and 77 km and is mainly due to drag uncertainty associated with the sphere descent that has a big impact during the transition from super to sub-sonic at these altitudes. Thus, 18 Jan 1990, the LiDAR detected the MIL bottom at around 65 km, while the falling sphere temperature profiles exhibit the MIL bottom higher near 68 km. However, the bottom of the MIL observed by the LiDAR corresponds better to the altitude where zonal and meridional winds start to decrease. Furthermore, the temperature profile from the falling spheres possesses a noise not realistic between 30 and 40 km, caused by an effect of vertical winds (Lübken et al., 1994), that is absent in the LiDAR profile. Therefore, to characterize mesospheric inversions with minimum uncertainty, only the temperature profiles acquired from Rayleigh LiDAR during the DYANA campaign are used to compute MIL's temperature amplitudes.

On the other hand, we notice that the ERA5 reanalyses imprecisely simulated the magnitude, thickness, and altitude of the temperature inversion for these two dates. Surprisingly, for both dates, the zonal and meridional winds deceleration processes associated with the MIL are simulated with quite realistic magnitudes in ERA5 but starting at lower altitudes that in spheres' observations.

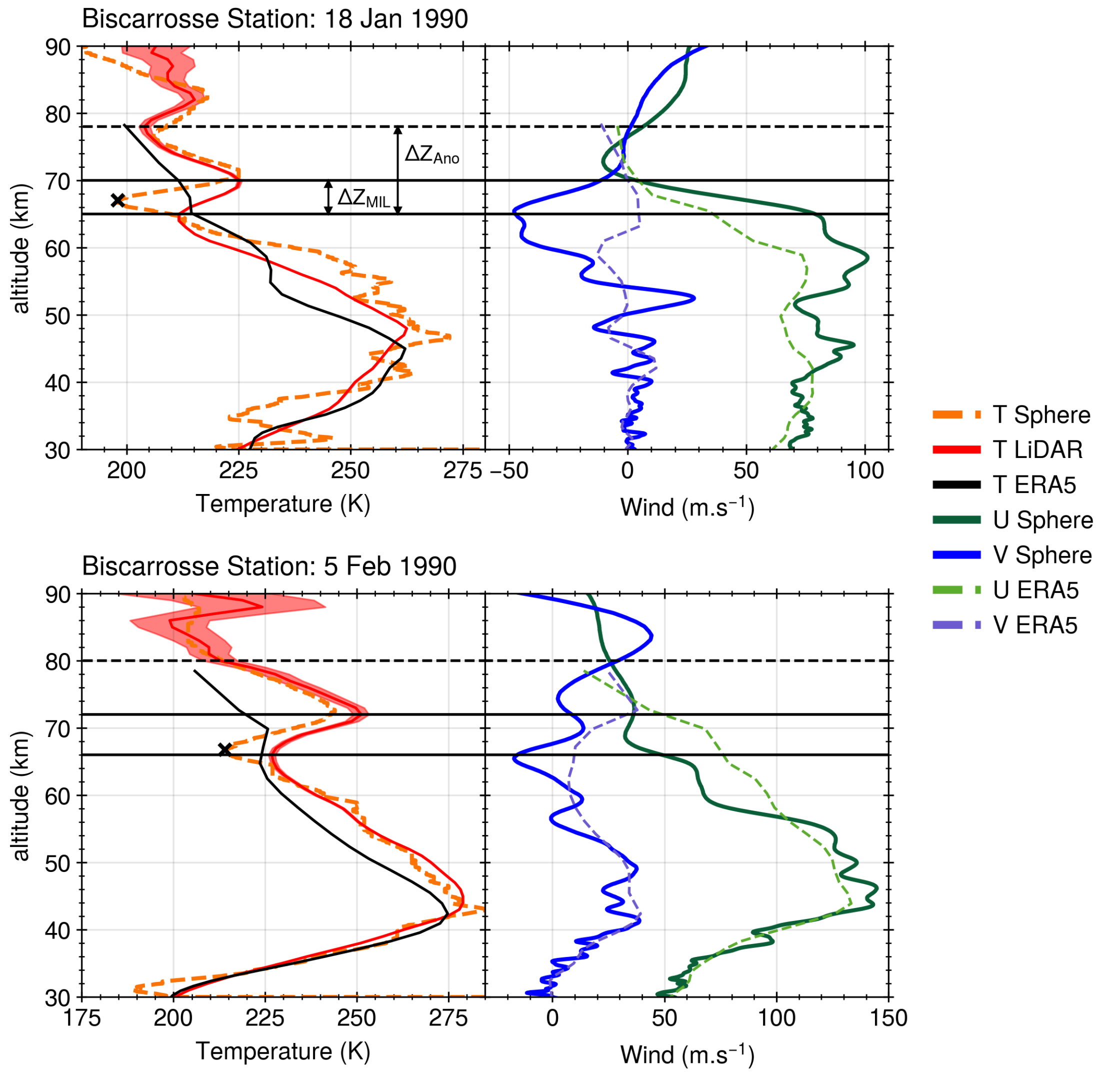

Figure 1. Temperature and wind profiles measured at Biscarrosse from falling spheres and Rayleigh LiDAR between 30 and 90 km for two dates during the DYANA Campaign. The statistical noise (red shaded area) of the LiDAR temperature signal is displayed. The two horizontal black solid lines indicate, respectively, the derived bottom and top of the MIL detected by the Rayleigh LiDAR. The horizontal dashed line represents the altitude of the potential total extension of the temperature anomaly (ΔZ_{Ano}). The black cross points out the bottom of the MIL measured from falling spheres. In addition, the ERA5 temperature-wind profiles extracted for each date are shown.

4.2 AboVE-2 campaign at OHP

After to have applied the MIL identification method to the 44 available temperature profiles, we found only four cases during the 2021/2022 winter in which a lower MIL was identifiable. In the mesosphere lidar wind measurements are challenging and depend on sky transparency, therefore, many actual wind observations suffer from weak signals, limiting accurate detection of lower MILs during this period. For the recent observations, only zonal wind measurements were performed by the Doppler LiDAR during the 2021/2022 winter to facilitate the inter-comparisons with the collocated Aeolus observations which measures essentially the zonal component of winds. Nevertheless, as the zonal wind is often larger than the meridional wind in the mesosphere by a factor of 10, we supposed that a zonal wind reduction implies very likely a total wind deceleration.

Figure 2 shows temperature and zonal wind profiles observed above the OHP for these four dates in the mesosphere where lower MILs were detected. Similar zonal wind deceleration behavior, as observed in Figure 1, is found within the lower MILs. Additionally, the altitudes at which the temperature starts to increase match well with those where the zonal wind starts to decelerate similarly to previous observations (Fig. 1) confirming the temperature-wind interconnection. Afterward, we computed the MIL's characteristics as described in section 3 for these four MIL events. For instance, on 3 Dec 2021, the MIL detected was characterized by a temperature elevation of 11.1 $\pm$ 3.9 K associated with a zonal wind deceleration of 43.3 $\pm$ 17 m.s^{-1}. However, since the zonal wind dropped over a larger altitude range than the one where the temperature increased, this computed zonal wind fluctuation is lower than the one observed which is in reality around 150 m.s^{-1} (Fig. 2). Consequently, as already mentioned above, these computed zonal wind amplitudes possess uncertainties due to the methodological conditions. These results also illustrate the Doppler LiDAR's capacity to capture strong wind fluctuations over narrow layers, as observed on 6 Dec 2021, where we computed, over a layer of 1.65 km, a zonal wind deceleration of 105.5 $\pm$ 57.5 m.s^{-1} associated with a temperature elevation of 29.5 $\pm$ 19.2 K. Finally, the MIL events on 12 Dec 2021, with a temperature elevation of 6.5 $\pm$ 2.9 K associated with a zonal wind drop of 34.3 $\pm$ 10.1 m.s^{-1}, while on 31 Jan 2022, with a temperature elevation of 46.8 $\pm$ 14.3 K associated with a zonal wind deceleration of 59.4 $\pm$ 68.7 m.s^{-1}, show, unlike above Biscarrosse, that large temperature amplitudes within MILs tend to be directly related to substantial wind deceleration (see Fig. 3). Thus, over these six MIL events, we found a mean temperature gradient of 7.5 K.km^{-1} associated with a mean zonal wind deceleration gradient of 21 m.s^{-1}.km^{-1}.

On 3 Dec 2021, a second MIL was present at 75 km in the temperature profile but the altitude range of the wind observations at this altitude do not allow to derive wind deceleration of this MIL. Despite this inherent uncertainty, the Doppler LiDAR technique appears to be an excellent instrument for documenting MIL's effects on winds. Finally, unlike the two MILs above Biscarrosse, ERA5 reanalyses, whether temperature or wind, did not reproduce MILs' presences for these four dates above the OHP.

5 Discussion and perspectives on mechanisms responsible for lower MILs

Given these new investigations of co-located temperature and wind observations in the mesosphere during MIL events (Figures 1 and 2), we can observe that MIL's formation involved systematic wind drops within the altitude range where the temperature increases. Figure 3 shows this interconnection between the zonal wind and the temperature for the six MIL events studied here where, interestingly, four cases appear aligned suggesting the existence of a positive correlation between these two variations. However, the two remaining cases depict a different behavior which can be due to several reasons such as observations carried out aside of the MIL center, other geophysical processes or

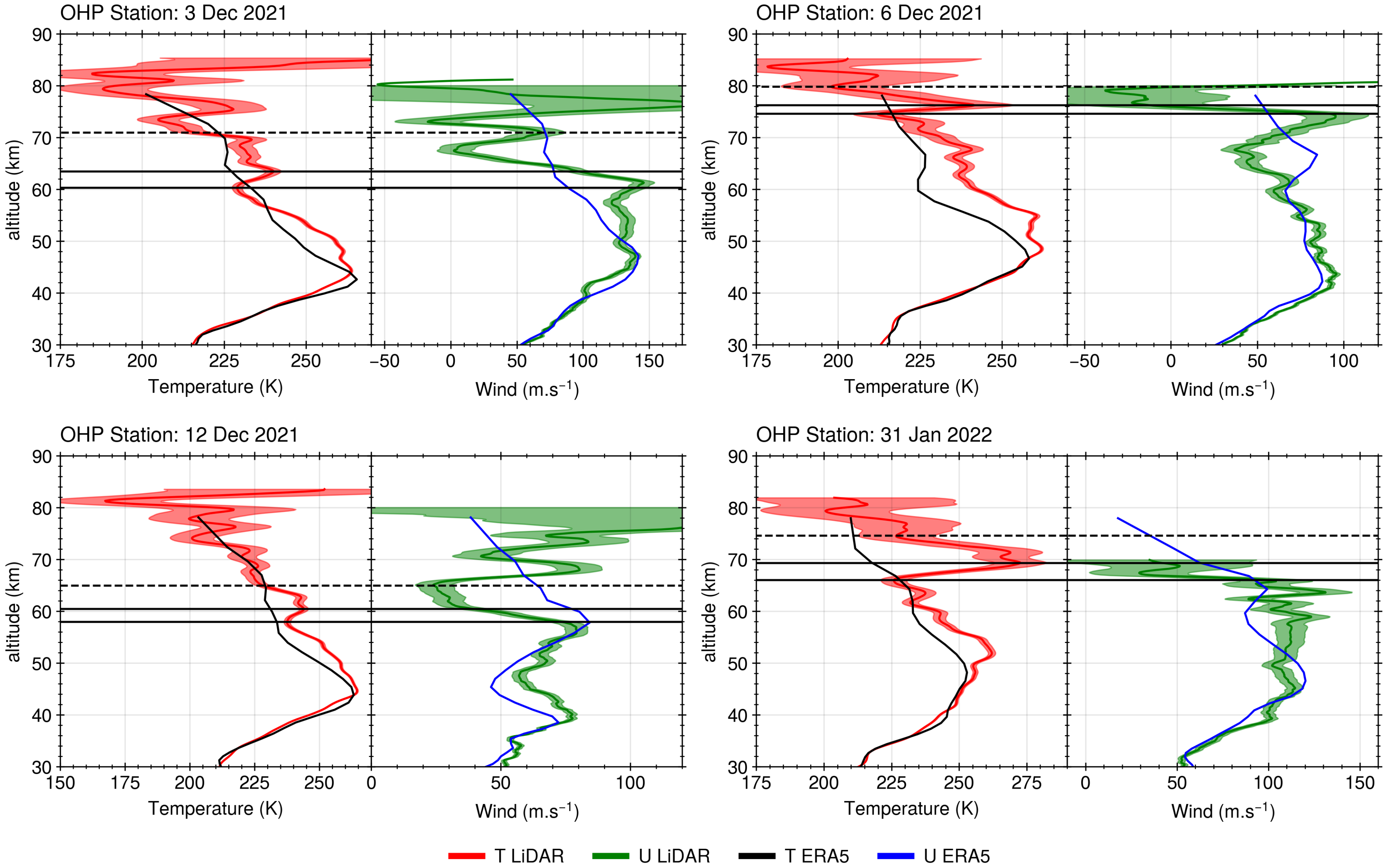

Figure 2. Temperature (red) and zonal wind (green) profiles measured for four dates in 2021/2022 winter from the Ozone LiDAR (temperature mode) and the Doppler LiDAR, respectively, located at the OHP. The statistical noise (shaded area) associated with these profiles is displayed. The three horizontal black lines indicate the same MIL's features that in Figure 1. Additionally, ERA5 temperature (black) and wind (blue) reanalyses profiles are shown for these four dates.

the employed method to compute wind shears. In the end, to lift these uncertainties, further temperature-wind observations are required.

Among the reported existing mechanisms, this observed connection between temperature and wind argues in the way of the MIL's formation mechanism as first introduced by Hauchecorne and Maillard (1990) who have simulated a temperature inversion by the breaking of gravity waves inside and above the MIL. In this simulation, the gravity wave dissipation occurs in a well-defined region where the associated momentum transfer decreases wind above the mesospheric jet, generating turbulence. The critical layer from which the zonal wind starts to decelerate appears when the wave phase speed is similar to the background wind. Then, the MIL is maintained with two processes: the heating due to viscous dissipation of turbulent motions and the downward vertical heat flux from the upper layer due to the turbulent vertical mixing in order to homogenize the potential temperature. Following the same aim, Sassi et al. (2002) have simulated a lower MIL between 70 and 80 km at mid-latitudes with the breaking of planetary waves, which generates warming in the upper stratosphere and cooling in the lower mesosphere favorable towards MIL's appearance. Their analysis has also shown that such lower MIL event occurs in a weak westward wind region produced by the deposition of momentum from westward gravity waves known to occur above 70 km (Mzé et al., 2014). Additionally, when they remove the gravity wave activity in their model, the positive temperature lapse rate created in the mesosphere disappears, confirming the crucial role of gravity waves in the lower MIL's formation and persistence.

Regarding the ERA5 capacity to reproduce the MIL's impact on the temperature and winds, Figure 1 shows that the ECMWF model is able, sometimes, to simulate the wind deceleration phenomenon with similar magnitude than the observations reported here while the temperature inversion is nearly overlooked. Nevertheless, for most cases, particularly over the OHP, Figure 2 shows that ERA5 reanalyses did not capture temperature and wind fluctuations in the mesosphere during MIL events. As already discussed in Mariaccia et al. (2022), who suggested that, first, the coarse vertical resolution of the model at these altitudes prevent the simulation of such fluctuations, and also, enhanced by the lack of assimilated observation by the model at these altitudes. Additionally, the sponge layer implemented in the model probably damps the gravity wave energy propagation up to the mesosphere which is necessary for MIL's apparition and sustainability. The realistic MIL characteristics statistics simulated by the Whole Atmosphere Community Climate Model (WACCM), benefiting from a better vertical resolution in the mesosphere than ERA5 (France et al., 2015), suggests that this is the first crucial step in the MIL's simulation achievement. Hence, according to these new observations, these suggested MIL's formation mechanisms should be considered as a first lead to pursue the elaboration of an accurate theory on the lower MIL's apparition. Future investigations are necessary to test how the energy transfer from gravity wave dissipation can create such background wind drop and temperature increase in the mesosphere. The elaboration of a new 3-D mechanistic model, in the same manner, that the one developed by Hauchecorne and Maillard (1990) should be pursued but with a better vertical resolution, to simulate temperature inversions by reducing locally wind.

On the other hand, regarding the LiDAR temperature profiles, as expected, the instrumental error associated with the Rayleigh LiDAR grow less quickly than for the Ozone LiDAR which is an expected result as this latter was not designed for measuring temperature. On the same aspects, the Doppler LiDAR observations still suffer of large instrumental errors in the higher mesosphere impacting the study of MIL's effects on zonal wind. Therefore, in order to improve our description of the MIL phenomenon, more wind observations performed by LIOwind Doppler LiDAR with meridional winds are required in addition to temperature measurements to benefit more extensive statistics of simultaneous wind temperature. Furthermore, the improvement of this technique to reduce instrumental errors in the upper mesosphere should be pursued. Finally, the develop-

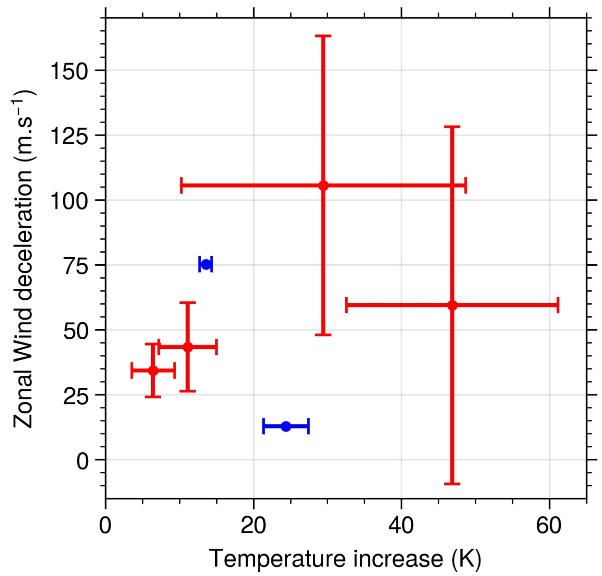

Figure 3. Zonal wind deceleration associated with their temperature increase for the six MIL events identified above Biscarrosse (in blue) and the OHP (in red). The errors associated with each computed value are shown as well.

ment of technical instruments capable of measuring the turbulence generated by gravity waves within MILs should be undertaken (Hauchecorne et al., 2016).

Open Research

The OHP ground-based lidar data can be obtained via NDACC lidar database `https://ndacc.larc.nasa.gov/`. The indications to download the ERA-5 data over 137 levels are given on the ECWMF website `https://confluence.ecmwf.int/display/CKB/How+to+download+ERA5`.

Acknowledgments

We gratefully thank the personnel of Station Gerard Megie at OHP (Frederic Gomez, Francois Dolon, Francois Huppert and others) for conducting the lidar observations. The work related to Aeolus validation has been performed in the frame of Aeolus Scientific Calibration & Validation Team (ACVT) activities under support of CNES Aeolus project. The temperature measurements have been obtained as part of as part of the Network for the Detection of Atmospheric Composition Change (NDACC). The falling sphere data as well as the lidar data from Centre d'Essai des Landes (CEL) have been acquired in the frame of the DYANA camapign implying Direction Générale de l'Armement (DGA). This work was performed within the framework of the European ARISE project and was funded by the French Educational Ministry with EUR IPSL.

References

Ardalan, M., Keckhut, P., Hauchecorne, A., Wing, R., Meftah, M., & Farhani, G. (2022). Updated climatology of mesospheric temperature inversions detected by rayleigh lidar above observatoire de haute provence, france, using a k-mean clustering technique. *Atmosphere*, *13*(5). doi: 10.3390/atmos13050814

Baumgarten, G. (2010). Doppler rayleigh/mie/raman lidar for wind and temperature measurements in the middle atmosphere up to 80 km. *Atmospheric Measurement Techniques*, *3*(6), 1509–1518. doi: 10.5194/amt-3-1509-2010

Chanin, M.-L., Garnier, A., Hauchecorne, A., & Porteneuve, J. (1989). A doppler lidar for measuring winds in the middle atmosphere. *Geophysical research letters*, *16*(11), 1273–1276.

Cutler, L. J., Collins, R. L., Mizutani, K., & Itabe, T. (2001). Rayleigh lidar observations of mesospheric inversion layers at poker flat, alaska (65 n, 147 w). *Geophysical research letters*, *28*(8), 1467–1470.

Dao, P. D., Farley, R., Tao, X., & Gardner, C. S. (1995). Lidar observations of the temperature profile between 25 and 103 km: Evidence of strong tidal perturbation. *Geophysical research letters*, *22*(20), 2825–2828.

Duck, T. J., Sipler, D. P., Salah, J. E., & Meriwether, J. W. (2001). Rayleigh lidar observations of a mesospheric inversion layer during night and day. *Geophysical Research Letters*, *28*(18), 3597–3600.

Engler, N. A. (1965). *Development of methods to determine winds, density, pressure, and temperature from the robin falling balloon.* (Tech. Rep.). DAYTON UNIV OHIO RESEARCH INST.

Fechine, J., Wrasse, C., Takahashi, H., Mlynczak, M., & Russell, J. (2008). Lower-mesospheric inversion layers over brazilian equatorial region using timed/saber temperature profiles. *Advances in Space Research*, *41*(9), 1447-1453. doi: https://doi.org/10.1016/j.asr.2007.04.070

France, J., Harvey, V., Randall, C., Collins, R., Smith, A., Peck, E., & Fang, X. (2015). A climatology of planetary wave-driven mesospheric inversion layers in the extratropical winter. *Journal of Geophysical Research: Atmospheres*, *120*(2), 399–413.

Gan, Q., Zhang, S. D., & Yi, F. (2012). Timed/saber observations of lower mesospheric inversion layers at low and middle latitudes. *Journal of Geophysical Research: Atmospheres*, *117*(D7).

Garnier, A., Chanin, M. L., Hauchecorne, A., & Porteneuve, J. C. (1992). *Laser device for measuring wind speeds at medium altitudes by using a doppler effect.* (US Patent 5,088,815)

Godin-Beekmann, S., Porteneuve, J., & Garnier, A. (2003). Systematic dial lidar monitoring of the stratospheric ozone vertical distribution at observatoire de haute-provence (43.92 n, 5.71 e). *Journal of environmental Monitoring*, *5*(1), 57–67.

Hauchecorne, A., Chanin, M.-L., & Keckhut, P. (1991). Climatology and trends of the middle atmospheric temperature (33–87 km) as seen by rayleigh lidar over the south of france. *Journal of Geophysical Research: Atmospheres*, *96*(D8), 15297–15309.

Hauchecorne, A., Chanin, M. L., & Wilson, R. (1987). Mesospheric temperature inversion and gravity wave breaking. *Geophysical Research Letters*, *14*(9), 933-936. doi: https://doi.org/10.1029/GL014i009p00933

Hauchecorne, A., Cot, C., Dalaudier, F., Porteneuve, J., Gaudo, T., Wilson, R., ... Besson, C. (2016, May). Tentative detection of clear-air turbulence using a ground-based rayleigh lidar. *Appl. Opt.*, *55*(13), 3420–3428. Retrieved from `https://opg.optica.org/ao/abstract.cfm?URI=ao-55-13-3420` doi: 10.1364/AO.55.003420

Hauchecorne, A., & Maillard, A. (1990). A 2-d dynamical model of mesospheric temperature inversions in winter. *Geophysical Research Letters*, *17*(12), 2197-2200. doi: https://doi.org/10.1029/GL017i012p02197

Hersbach, H., Bell, B., Berrisford, P., Hirahara, S., Horányi, A., Muñoz-Sabater, J., ... others (2020). The era5 global reanalysis. *Quarterly Journal of the Royal Meteorological Society*, *146*(730), 1999–2049.

Huang, T.-Y., Hickey, M. P., Tuan, T.-F., Dewan, E. M., & Picard, R. H. (2002). Further investigations of a mesospheric inversion layer observed in the aloha-93 campaign. *Journal of Geophysical Research: Atmospheres*, *107*(D19), ACL 17-1-ACL 17-8. doi: https://doi.org/10.1029/2001JD001186

Huang, T. Y., Hur, H., Tuan, T. F., Li, X., Dewan, E. M., & Picard, R. H. (1998). Sudden narrow temperature-inversion-layer formation in aloha-93 as a critical-layer-interaction phenomenon. *Journal of Geophysical Research: Atmospheres*, *103*(D6), 6323-6332. doi: https://doi.org/10.1029/97JD03076

Jones, L. M., & Peterson, J. W. (1968). Falling sphere measurements, 30 to 120 km. In R. S. Quiroz (Ed.), *Meteorological investigations of the upper atmosphere: Proceedings of the american meteorological society symposium on meteorological investigations above 70 kilometers, miami beach, florida, 31 may–2 june 1967* (pp. 176–189). Boston, MA: American Meteorological Society. doi: 10.1007/978-1-935704-37-9_21

Khaykin, S. M., Hauchecorne, A., Wing, R., Keckhut, P., Godin-Beekmann, S., Porteneuve, J., ... Schmitt, J. (2020). Doppler lidar at observatoire de haute-provence for wind profiling up to 75 km altitude: performance evaluation and observations. *Atmospheric Measurement Techniques*, *13*(3), 1501–1516. doi: 10.5194/amt-13-1501-2020

Leblanc, T., & Hauchecorne, A. (1997). Recent observations of mesospheric temperature inversions. *Journal of Geophysical Research: Atmospheres*, *102*(D16), 19471–19482.

Leblanc, T., Hauchecorne, A., Chanin, M.-L., Rodgers, C., Taylor, F., & Livesey, N. (1995). Mesospheric temperature inversions as seen by isams in december 1991. *Geophysical research letters*, *22*(12), 1485–1488.

Leblanc, T., McDermid, I. S., Keckhut, P., Hauchecorne, A., She, C. Y., & Krueger, D. A. (1998). Temperature climatology of the middle atmosphere from long-term lidar measurements at middle and low latitudes. *Journal of Geophysical Research: Atmospheres*, *103*(D14), 17191-17204. doi: https://doi.org/10.1029/98JD01347

Le Du, T., Keckhut, P., Hauchecorne, A., & Simoneau, P. (2022). Observation of gravity wave vertical propagation through a mesospheric inversion layer. *Atmosphere*, *13*(7). Retrieved from `https://www.mdpi.com/2073-4433/13/7/1003` doi: 10.3390/atmos13071003

Liu, H.-L., & Hagan, M. E. (1998). Local heating/cooling of the mesosphere due to gravity wave and tidal coupling. *Geophysical Research Letters*, *25*(15), 2941–2944.

Lübken, F.-J., Hillert, W., Lehmacher, G., Zahn, U., Bittner, M., Offermann, D., ... Czechowsky, P. (1994). Intercomparison of density and temperature profiles obtained by lidar, ionization gauges, falling spheres, datasondes and radiosondes during the dyana campaign. *Journal of Atmospheric and Terrestrial Physics*, *56*(13), 1969-1984. (Dynamic Adapted Network for the the Atmosphere) doi: https://doi.org/10.1016/0021-9169(94)90023-X

Mariaccia, A., Keckhut, P., Hauchecorne, A., Claud, C., Le Pichon, A., Meftah, M., & Khaykin, S. (2022). Assessment of era-5 temperature variability in the middle atmosphere using rayleigh lidar measurements between 2005 and 2020. *Atmosphere*, *13*(2), 242.

Meriwether, J. W., & Gardner, C. S. (2000). A review of the mesosphere inversion layer phenomenon. *Journal of Geophysical Research: Atmospheres*, *105*(D10), 12405–12416.

Meriwether, J. W., & Gerrard, A. J. (2004). Mesosphere inversion layers and stratosphere temperature enhancements. *Reviews of Geophysics*, *42*(3). doi: https://doi.org/10.1029/2003RG000133

Meriwether, J. W., & Mlynczak, M. G. (1995). Is chemical heating a major cause of the mesosphere inversion layer? *Journal of Geophysical Research: Atmospheres*, *100*(D1), 1379–1387.

Mzé, N., Hauchecorne, A., Keckhut, P., & Thétis, M. (2014). Vertical distribution of gravity wave potential energy from long-term rayleigh lidar data at a northern middle-latitude site. *Journal of Geophysical Research: Atmospheres*, *119*(21), 12,069-12,083. doi: https://doi.org/10.1002/2014JD022035

Offermann, D. (1994). The dyana campaign: a survey. *Journal of Atmospheric and Terrestrial Physics*, *56*(13), 1639-1657. (Dynamic Adapted Network for the the Atmosphere) doi: https://doi.org/10.1016/0021-9169(94)90002-7

Ramesh, K., Sridharan, S., & Vijaya Bhaskara Rao, S. (2013). Dominance of chemical heating over dynamics in causing a few large mesospheric inversion layer events during january–february 2011. *Journal of Geophysical Research: Space Physics*, *118*(10), 6751–6765.

Ratynski, M., Khaykin, S., Hauchecorne, A., Wing, R., Cammas, J.-P., Hello, Y., & Keckhut, P. (2022). Validation of aeolus wind profiles using ground-based lidar and radiosonde observations at la réunion island and the observatoire de haute provence. *EGUsphere*, *2022*, 1–33. doi: 10.5194/egusphere-2022-822

Salby, M., Sassi, F., Callaghan, P., Wu, D., Keckhut, P., & Hauchecorne, A. (2002). Mesospheric inversions and their relationship to planetary wave structure. *Journal of Geophysical Research: Atmospheres*, *107*(D4), ACL 4-1-ACL 4-13. doi: https://doi.org/10.1029/2001JD000756

Sassi, F., Garcia, R. R., Boville, B. A., & Liu, H. (2002). On temperature inversions and the mesospheric surf zone. *Journal of Geophysical Research: Atmospheres*, *107*(D19), ACL 8-1-ACL 8-11. doi: https://doi.org/10.1029/2001JD001525

Schmidlin, F. (1976). Temperature inversions near 75 km. *Geophysical Research Letters*, *3*(3), 173–176.

Souprayen, C., Garnier, A., Hertzog, A., Hauchecorne, A., & Porteneuve, J. (1999, Apr). Rayleigh–mie doppler wind lidar for atmospheric measurements. i.

instrumental setup, validation, and first climatological results. *Appl. Opt.*, *38*(12), 2410–2421. doi: 10.1364/AO.38.002410

Straume, A.G., Rennie, M., Isaksen, L., de Kloe, J., Marseille, G.-J., Stoffelen, A., ... Parinello, T. (2020). Esa´s space-based doppler wind lidar mission aeolus - first wind and aerosol product assessment results. *EPJ Web Conf.*, *237*, 01007. doi: 10.1051/epjconf/202023701007

Stroud, W. G., Nordberg, W., Bandeen, W. R., Bartman, F. L., & Titus, P. (1960). Rocket-grenade measurements of temperatures and winds in the mesosphere over churchill, canada. *Journal of Geophysical Research (1896-1977)*, *65*(8), 2307-2323. doi: https://doi.org/10.1029/JZ065i008p02307

Theon, J. S., Nordberg, W., Katchen, L. B., & Horvath, J. J. (1967). Some observations on the thermal behavior of the mesosphere. *Journal of Atmospheric Sciences*, *24*(4), 428 - 438. doi: 10.1175/1520-0469(1967)024⟨0428:SOOTTB⟩2.0.CO;2

Wing, R., Hauchecorne, A., Keckhut, P., Godin-Beekmann, S., Khaykin, S., McCullough, E. M., ... d'Almeida, E. (2018). Lidar temperature series in the middle atmosphere as a reference data set–part 1: Improved retrievals and a 20-year cross-validation of two co-located french lidars. *Atmospheric Measurement Techniques*, *11*(10), 5531–5547.

Wing, R., Martic, M., Hauchecorne, A., Porteneuve, J., Keckhut, P., Courcoux, Y., ... Cocuron, D. (2020). Atmospheric density and temperature vertical profile retrieval for flight-tests with a rayleigh lidar on-board the french advanced test range ship monge. *Atmosphere*, *11*(1). doi: 10.3390/atmos11010075